DOI: 10.21062/mft.2025.037 © 2025 Manufacturing Technology. All rights reserved. http://www.journalmt.com

Influence of Surface Preparation on XRD Peak Parameters and Residual Stress Measurements

Pavel Salvetr (0000-0001-5717-267X)[1], Aleksandr Gokhman (0000-0002-0533-2114)[2], Jan Drahokoupil (0000-0003-0855-5142)[3]
[1]COMTES FHT. Průmyslová 995, 334 41 Dobřany. Czech Republic. E-mail: pavel.salvetr@comtesfht.cz
[2]Department of Physics, South Ukrainian National Pedagogical University (SUNPU). Staroprotfrankivska 26, 65020 Odessa. Ukraine. E-mail: alexander.gokhman@gmail.com
[3]FZU – The Institute of Physics of the Czech Academy of Sciences, Na Slovance 1999/2, Prague 8, 182 21, Czech Republic. E-mail: draho@fzu.cz

X-ray diffraction (XRD) is an analytical technique used to investigate the crystal structure properties of materials. However, the accuracy of XRD measurements can be significantly affected by the sample's surface preparation. This study evaluates the impact of various surface preparation methods on the diffraction peak characteristics, phase composition, and residual stress analysis of two metallic materials: very low-alloyed iron-based alloy labelled as pure iron and hardened 54SiCr6 steel. Various final steps of metallographic preparation of the surface for XRD were used, including mechanical grinding with coarse (P120) and fine (P1200) sandpapers, polishing with OPS colloidal silica, chemical etching in hot hydrochloric acid, and electrolytic etching. The results show that surface conditions influence the full width at half maximum (FWHM) more than the intensity of diffraction peaks. Furthermore, the annealed pure iron sample (with low hardness) exhibited a more pronounced sensitivity to surface preparation compared to hardened 54SiCr6 steel, with its martensitic microstructure. Residual stress analysis using the $\sin^2\psi$ method further revealed that mechanical grinding induces substantial compressive residual stress while polishing and etching methods produce nearly neutral, or slightly tensile, residual stresses. These findings highlight the importance of consistent and appropriate surface preparation methods for reliable XRD analysis.

Keywords: XRD diffraction, Peak characteristics, Residual stress, Surface preparation, Dislocation density

1 Introduction

X-ray diffraction (XRD) is a widely used non-destructive analytical technique for the investigation of physical properties of materials. It is an essential tool for determining the crystal structures of inorganic metallic and non-metallic materials, organic compounds, and biological samples such as proteins and nucleic acids. XRD is also utilized in the pharmaceutical industry, where it is employed to analyze the polymorphism and chirality of active pharmaceutical ingredients [1,2]. The technique is suitable for studying single crystals and polycrystalline materials, including powdered and compact samples. Compact samples require a flat surface for accurate analysis. The principle of XRD involves exposing the sample to monochromatic X-ray radiation. As the X-rays penetrate the sample, elastic scattering (diffraction) occurs at the atomic lattice planes. The direction and intensity of the diffracted beams are determined by the internal structure of the sample. When X-rays interact with a crystal (a periodically repeating structure), constructive interference occurs in specific directions, provided Bragg's law (Eq. 1) is satisfied, where n is the order of diffraction, λ is the X-ray beam wavelength, d is the interplanar spacing, and θ is the diffraction angle between the X-Ray beam and crystal surface. In all other directions, the reflections cancel out, and the X-ray beams are extinguished [3].

$$n\lambda = 2d \sin\theta \quad (1)$$

X-ray diffraction (XRD) provides critical insights into the internal structure of materials, such as lattice parameters, space groups, atomic positions within the unit cell, preferred orientation of planes (texture), crystallite size (coherently diffracting domains), microstrain, residual stresses, and thickness measurements of thin films and coatings. For multiphase mixtures, XRD enables qualitative and quantitative phase analysis, including the evaluation of amorphous phase content. Knowledge of residual stresses in a material is crucial for preventing crack formation [4]. Residual stresses change during heat treatment, machining, or material joining [5], and they can also indicate the emergence of defects within the material [6]. Key characteristics of diffraction lines analyzed in XRD include intensity (peak height), width commonly expressed as full width at half maximum (FWHM) and position of the diffraction line [3].

It is important to note that, in the context of metallic materials research, XRD should be considered a surface sensitive technique with an effective penetration depth of a few tens of micrometers usually, depending on the chemical composition and density of the investigated specimen, the energy (wavelength) of the X-ray radiation used, and the incident and diffracted angles. Additionally, the radiation is exponentially attenuated in matter [7]. Thus, the surface condition of the analyzed sample has a significant impact on the results obtained from XRD measurements.

The main aim of this study is to describe the influence of surface preparation on the key characteristics of diffraction lines of metallic materials, specifically steel samples. Metallic materials undergo numerous technological processes (such as casting and solidification, forming, heat treatment involving recrystallization processes and phase transformations, and machining operations) that enable their final application while leaving a fingerprint on their crystal structure. XRD is generally used to measure phase composition rapidly. However, additional results derived from XRD data – such as dislocation density, microstrain [8], and residual stress are highly sensitive to the condition of the analyzed surface. In literature, the experimental part sometimes lacks a detailed description of the surface preparation process for XRD analysis [9]. In some cases, mechanically polished surfaces are used [10], or mechanically polished surfaces with the top layer etched off in an acid solution [11–13] or the surface layer is removed during chemical polishing [14]. Electrolytic polishing is suitable as the final step of sample preparation, commonly used for measuring the depth profile of residual stresses [15,16].

The procedure for determining the amount of retained austenite in steels is described in the ASTM E975[17], which specifies standard metallographic sample preparation consisting of wet grinding (using abrasive papers with silicon carbide or aluminium oxide particles) followed by final polishing with 6 μm aluminium oxide particles or an equivalent abrasive polish. Electrolytic or chemical polishing may also be used. Conversely, etching with hot acid is not recommended, as it may cause selective etching of one phase or along a preferred crystallographic direction.

The hypothesis is that samples with different mechanical properties and resistance to plastic deformation represented by hardness values will exhibit varying sensitivity to surface preparation in terms of its effect on XRD data. Therefore, in this study, two iron-based alloys with differing microstructures and hardness were investigated.

2 Materials and Methods

Two experimental materials were investigated in this study. The first material was a very low-alloy steel (referred to as pure iron). The heat treatment of this material consisted of annealing at 700 °C for 4 hours, followed by slow cooling in a furnace. The second experimental material was hardened 54SiCr6 steel. The heat treatment for this material was designed to achieve the highest possible hardness, involving austenitization at 900 °C for 20 minutes, followed by oil quenching. The chemical compositions of the experimental materials are given in Tab. 1.

Tab. 1 *Chemical composition of investigated materials*

Sample (wt.%)	C	Si	Mn	Cr	Mo	Ni	Cu	Fe
54SiCr6	0.55	1.51	0.71	0.79	0.055	0.108	0.04	Bal.
Pure Fe	<0.0003	<0.0005	0.04	0.006	0.004	0.004	0.01	

The microstructure was observed by the optical microscope Nikon Eclipse MA200 (light microscope, (LM) (Nikon, Tokyo, Japan). The microstructure was revealed by etching with 2% Nital reagent. The hardness was determined using an automatic Vickers hardness tester under a load of 10 kg for 10 seconds, following the ČSN EN ISO 6507-1 standard. The surface roughness of the samples was measured using a Keyence VK-X3000 laser confocal microscope. The sample surfaces were captured with a 200x magnification objective and scanned with a laser. The surface roughness was measured five times per sample. The resulting surface roughness value, Sa, represents the average of these five measurements.

XRD analysis was performed using a Bruker D8 Discover diffractometer (Bruker AXS GmbH, Karlsruhe, Germany) with a copper anode (λ $K_{\alpha 1}$=0.15406 nm) operating at 40 kV and 40 mA, in Bragg-Brentano geometry. Measurements were carried out with a step size of 0.025° and a time per step of 0.25 s, within the 2θ range of 30–125°. XRD data were collected three times at different regions of the sample using polycapillary optics (2 mm diameter). Under these measurement conditions, the effective penetration depth, was calculated using the AbsorbDX tool in the DIFFRAC.EVA software, and is expected to range from 1.2 to 4.3 μm. The characteristics of the diffraction peaks, including intensity, position, and full width at half maximum (FWHM), were analyzed using Diffrac EVA software (Bruker AXS GmbH, Karlsruhe, Germany). The phase composition and lattice parameters were determined by Rietveld refinement using Topas software (Bruker AXS GmbH, Karlsruhe, Germany) [18].

The dislocation density of samples was calculated from XRD patterns using the modified Williamson-Hall (W-H) method. The basic equation of the modified W-H method is written as Eq. 2 [19]:

$$\Delta K = \left(\frac{0.9}{D}\right)^2 + \frac{\pi M b^2}{2}\,\rho^{\frac{1}{2}} K C^{\frac{1}{2}} \quad (2)$$

Where:

ρ…The dislocation density;

K…Denotes the magnitude of the diffraction vector, calculated as $K=2sin\theta/\lambda$;

θ, λ…Represent the diffraction angle and X-ray wavelength, respectively;

D…The crystallite size;

ΔK…Can be expressed as $\Delta K=2cos\theta(\Delta\theta)/\lambda$;

$\Delta\theta$…The FWHM;

The constant M is determined by the effective cut-off radius of dislocations [20]. The Burgers vector b is 0.248 nm. The dislocation contrast factor (C) for a given (hkl) diffraction peak is defined according to Eq. (3,4) [19]:

$$C = C_{h00}(1 - qH^2) \quad (3)$$

$$C_{h00} = \frac{h^2k^2 + h^2l^2 + k^2l^2}{(h^2 + k^2 + l^2)^2} \quad (4)$$

According to Eq. 2, ΔK can be regarded as a linear function of $KC^{1/2}$. By fitting data from at least five diffraction peaks, the dislocation density ρ can be calculated using the slope β:

$$\rho = \frac{2\beta}{\pi b^2 M^2} \quad (5)$$

The standard error of the slope β is obtained from the covariance matrix during the fitting process. This standard error quantifies the uncertainty in β and is then propagated through Eq. 5 to estimate the error in dislocation density ρ.

Residual stress was determined using the $\sin^2\psi$ method. The diffracted plane of ferrite (222) ($2\theta\approx137.3°$) was used for residual stress measurement. The measurements occurred with a 1 mm collimator within the 2θ range of 133–143° and a step size of 0.05°. A total of nine tilt angles were used, equidistantly ψ up to 80°, for directions with angles φ of 0°, 45°, and 90°. The used Young's modulus and Poisson ratio were 190 GPa and 0.29, respectively, assuming no texture in the material studied. The Leptos software (Bruker AXS GmbH, Karlsruhe, Germany) was used for residual stress calculations.

X-ray diffraction data were acquired for samples prepared with different surface conditions: after grinding with P120 and P1200 sandpapers, after polishing with a final step using OPS colloidal silica with a 0.05 μm particle size, after removal of the surface layer by etching in hydrochloric acid, and after electrolytic polishing using Struers Tegramin under the following conditions: duration of 3 min, applied voltage of 20 V, electrolyte Struers A2. A 50 μm thick surface layer was removed via electrolytic etching. This variation in surface preparation emphasizes the impact of surface conditions on the quality and accuracy of XRD measurements, as each preparation method influences the peak characteristics and the residual stress state of the surface in distinct ways.

3 Results and Discussion

3.1 Characterization of microstructure, hardness and surface roughness

The microstructure of the hardened 54SiCr6 steel sample consisted of martensite and retained austenite. The hardness reached the value of 767±4 HV10. On the contrary, the hardness of the pure iron sample was 82±1 HV10 and the microstructure consisted of recrystallized grains of ferrite, as shown in Fig. 1.

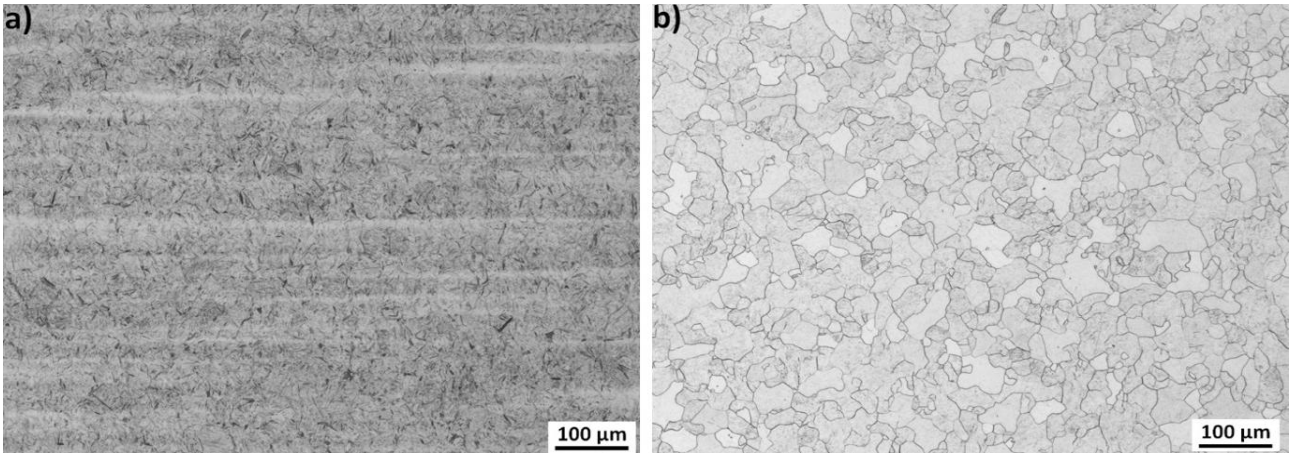

Fig. 1 *Microstructures of investigated samples a) martensitic microstructure of hardened 54SiCr6 steel b) ferritic grains in microstructure of pure Fe sample after annealing at 700 °C*

The surface roughness results indicate a clear influence of surface preparation methods on both the hardened 54SiCr6 steel and pure Fe samples. The highest surface roughness with an average peak height Sa=1.22 μm was measured for the electrolytic etched 54SiCr6 steel sample. In the case of mechanically ground and polished samples, finer abrasive and polishing particles reduced the surface roughness for both 54SiCr6 and pure Fe samples. Chemical etching with HCl produced comparable roughness levels for both materials, measuring 0.22 μm for 54SiCr6 and 0.27 μm for pure Fe sample, approximately twice the surface roughness of OPS-polished samples. After mechanical grinding with P120 and P1200 sandpapers, the hardened 54SiCr6 steel samples exhibited lower roughness values compared to the pure Fe samples, see Tab. 2.

Tab. 2 *Surface roughness of the hardened 54SiCr6 steel and pure Fe sample*

Sample	Surface condition	Sa (μm)
54SiCr6	P120	0.38 ± 0.03
54SiCr6	P1200	0.15 ± 0.01
54SiCr6	OPS	0.12 ± 0.01
54SiCr6	HCl	0.22 ± 0.01
54SiCr6	Electrolytic Etching	1.22 ± 0.08
Fe	P120	0.74 ± 0.08
Fe	P1200	0.27 ± 0.03
Fe	OPS	0.12 ± 0.01
Fe	HCl	0.27 ± 0.01
Fe	Electrolytic Etching	0.63 ± 0.05

3.2 XRD results

XRD patterns of both investigated materials are shown in Fig. 2. Diffraction peaks corresponding to ferrite/martensite planes (222) and retained austenite – planes (111), (200), (220), (311), (222), (400) and (311) – are visible in the hardened 54SiCr6 steel samples, whereas only ferrite peaks appear in the XRD pattern of the pure iron sample. When comparing the diffractograms of both samples, noticeable differences in peak shapes can be observed. The 54SiCr6 steel sample, which was hardened and contains more alloying elements, predominantly exhibits a martensitic microstructure. Martensite is a supersaturated solid solution of carbon in iron, which distorts the cubic BCC (Body-Centered Cubic) lattice into a BCT (Body-Centered Tetragonal) lattice, resulting in broad diffraction peaks. This broadening is attributed to the high concentration of lattice defects such as dislocations, vacancies, and interstitial atoms. In contrast, the diffraction peaks of ferrite are narrow, corresponding to recrystallized grains of ferrite with a minimal amount of crystal defects.

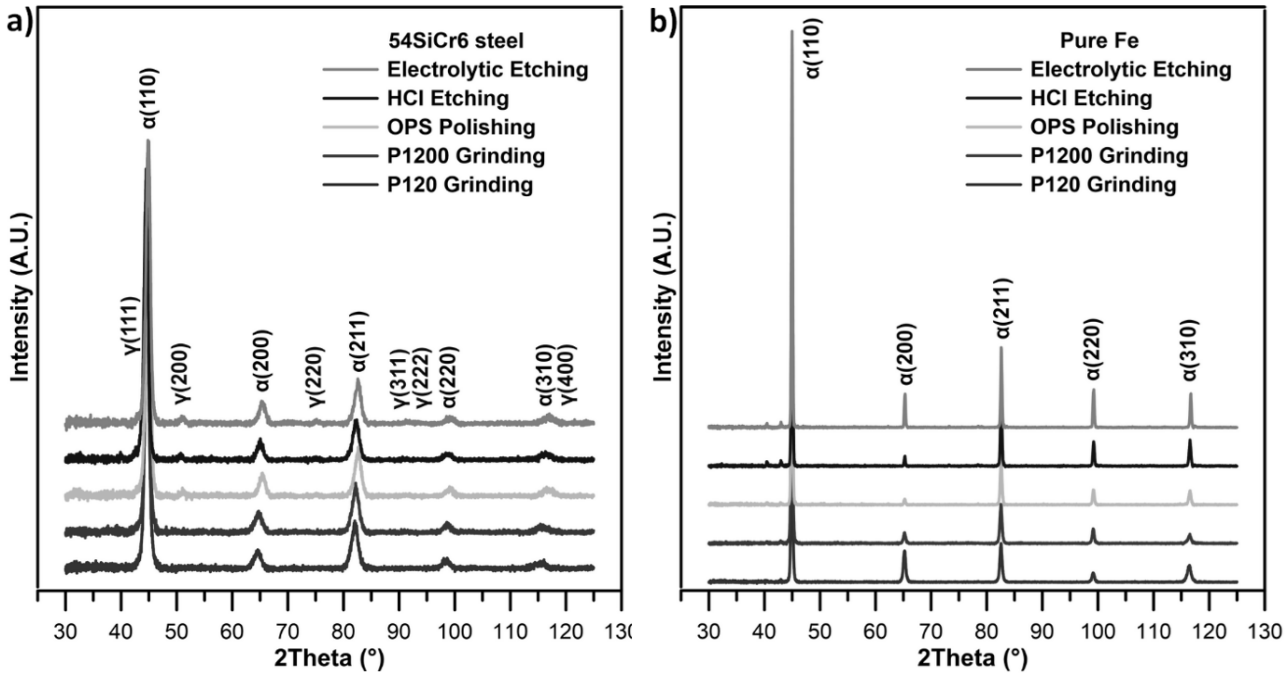

Fig. 2 *XRD patterns of a) hardened 54SiCr6 steel b) pure Fe sample after annealing at 700 °C*

Firstly, the phase composition and lattice parameters of the 54SiCr6 steel sample were evaluated using the TOPAS software. The peaks corresponding to diffraction planes of ferrite/martensite (110), (200), (211), (220), and (310) and retained austenite (111), (200), (220), (311), (222) and (400) were used. Because the diffraction peaks of ferrite (110) and austenite (111) overlap, the evaluation was also performed excluding these two peaks, starting from 2θ=48°. It is important to emphasize that the austenite peaks did not reach sufficient intensities for phase composition analysis after simple surface grinding using P120 and P1200 sandpapers. The content of retained austenite and lattice parameters are listed in Tab. 3. It is evident that the overlap of austenite (111) and ferrite (110) diffraction peaks has a significant impact on the phase composition results, while its effect on lattice parameters is lower. Without considering these two overlapping peaks, the retained austenite content ranged between 7 and 8.5 wt.%, whereas the analysis including the overlapping peaks indicated a higher retained austenite content of 11 wt.% to 16 wt.%. In the case of lattice parameter results, it is evident that the values are consistent for surfaces prepared by electrolytic etching and polishing with OPS colloidal silica as the final step. Slightly lower lattice parameters were observed for surfaces etched in HCl, whereas an increase in lattice parameters was recorded for surfaces prepared by grinding with P1200 and P120 sandpapers. For pure iron samples, only the lattice parameters of ferrite were evaluated. The differences between the various surface preparation methods are significantly smaller; however, a similar trend to that observed in the hardened 54SiCr6 steel can be noted. Samples prepared by electrolytic etching, etching in hydrochloric acid, and polishing with OPS colloidal silica exhibited lower lattice parameters, while samples prepared by mechanical grinding showed higher lattice parameters.

Tab. 3 *Phase composition and lattice parameters depending on the surface preparation method and used 2θ range*

2θ range	Sample	Surface	RA (wt.%)	a_{FCC} (Å)	$a_{BCC/BCT}$ (Å)	c_{BCT} (Å)
30-125°	54SiCr6	P120	x	x	2.8658 ± 0.0021	2.8922 ± 0.0037
	54SiCr6	P1200	x	x	2.8586 ± 0.0032	2.8896 ± 000.33
	54SiCr6	OPS	12.4 ± 1.4	3.5740 ± 0.0048	2.8483 ± 0.0029	2.8746 ± 0.0065
	54SiCr6	HCl	15.7 ± 1.2	3.5815 ± 0.0018	2.8533 ± 0.0067	2.8701 ± 0.0043
	54SiCr6	El. Et.	11.4 ± 0.7	3.5761 ± 0.0037	2.8488 ± 0.0072	2.8780 ± 0.0135
48-125°	54SiCr6	P120	x	x	2.8623 ± 0.0004	2.8865 ± 0.0044
	54SiCr6	P1200	x	x	2.8577 ± 0.0011	2.8881 ± 0.0004
	54SiCr6	OPS	7.0 ± 0.3	3.5761 ± 0.0037	2.8530 ± 0.0034	2.8758 ± 0.0065
	54SiCr6	HCl	7.6 ± 1.0	3.5834 ± 0.0014	2.8563 ± 0.0065	2.8708 ± 0.0043
	54SiCr6	El. Et.	8.5 ± 0.2	3.5573 ± 0.0001	2.8527 ± 0.0031	2.8781 ± 0.0088
30-125°	Pure Fe	P120	x	x	2.8673 ± 0.0001	x
	Pure Fe	P1200	x	x	2.8676 ± 0.0002	x
	Pure Fe	OPS	x	x	2.8668 ± 0.0001	x
	Pure Fe	HCl	x	x	2.8667 ± 0.0002	x
	Pure Fe	El. Et.	x	x	2.8659 ± 0.0004	x

Secondly, diffraction peak characteristics of FWHM and intensity were evaluated and compared for various surface and material states. Generally, the FWHM value of diffraction peaks is influenced by several factors, which can be broadly categorized into sample-related and instrumental effects. Sample-related factors include crystallite size, microstrain, lattice defects, dislocations, stacking faults, residual stresses, and surface preparation methods, all of which can disrupt the periodicity or integrity of the crystal lattice. The main instrumental factors are instrumental broadening caused by imperfections in the diffractometer setup, such as divergence of the X-ray beam, misalignment of optics, measurement conditions, and detector resolution and also, temperature effects involving e.g. thermal vibrations and lattice expansion. Instrumental factors and temperature effects can be neglected, as all measurements were conducted under the same diffractometer setup and at a constant temperature. The intensity of diffraction peaks in XRD is again influenced by numerous factors such as crystallographic orientation, crystallite size, phase composition, lattice defects, microstructure, absorption properties, surface preparation methods, measurement conditions, and the wavelength of the X-ray used. Factors such as texture and surface preparation method are relevant to this study primarily. Significant differences were observed between the hardened 54SiCr6 steel and pure iron samples in their response to surface preparation methods, particularly in the FWHM results. While for the pure Fe sample, FWHM values progressively increased for all diffraction peaks from samples electrolytically etched, etched in HCl, polished using OPS, ground with P1200 sandpaper, to finally grinding with

P120 sandpaper, the 54SiCr6 steel sample did not show a consistent trend for FWHM values across the different surface preparation methods. For example, the lowest FWHM value for the (220) peak was recorded for the sample ground with P120 sandpaper, as shown in Fig. 3. The intensity of diffraction peaks appears to be less sensitive to the surface preparation method compared to the FWHM values. Larger differences in peak intensities were observed for the main diffraction peak (110), while for other peaks, the differences were smaller. In the case of the hardened 54SiCr6 steel, the results for the remaining peaks were nearly identical, as shown in Fig. 3.

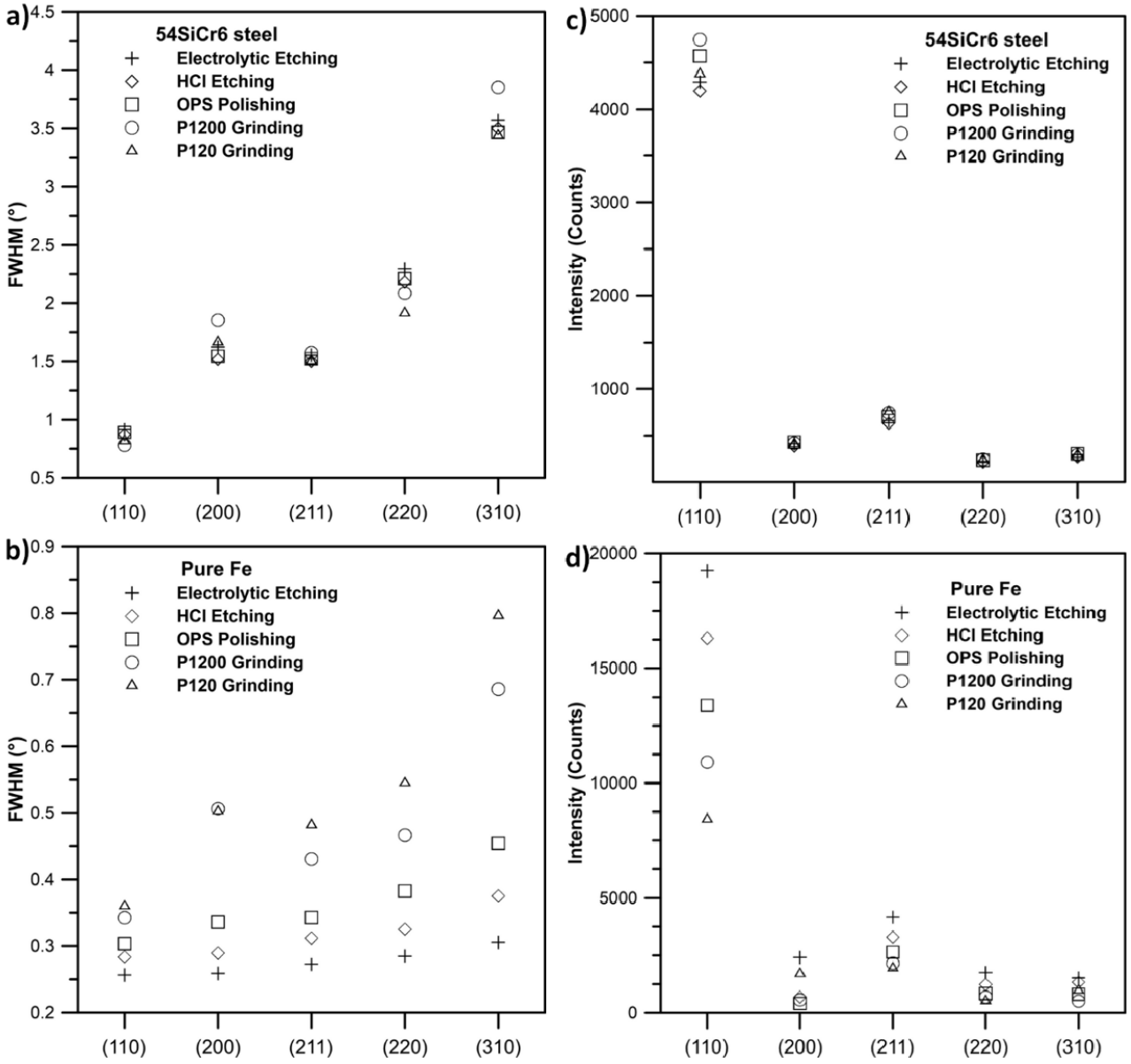

Fig. 3 *FWHM and intensities of diffraction peaks of a), c) hardened 54SiCr6 steel and b), d) pure Fe sample after annealing at 700 °C*

The results of calculating the dislocation density (ρ) using the modified W-H method for the material under study are presented in Tab. 4. To determine ρ, the XRD data on reflexes (110), (200), (211), (220) and (310) were used. A clear dependence of dislocation density on the sample polishing method for XRD measurement was observed for pure iron. Sandpaper with large abrasive particles causes significant deformation of the sample and increases the number of crystalline defects. This affected layer is gradually removed in subsequent polishing steps, resulting in a decrease in dislocation density. For hardened 54SiCr6 steel, a decrease in dislocation density was also found with changes in surface condition compared with P1200 grinding. However, for the steel under study, this effect is not as significant as for pure iron, since the dislocation density of the base (unaffected) 54SiCr6 steel was very high.

Tab. 4 *Dislocation density calculation using the modified W-H method*

Material	Electrolytic Etching	HCl Etching	OPS Polishing	P1200 Grinding	P120 Grinding
Pure iron	$(2.58\pm0.31)\cdot10^{11}$ m^{-2}	$(7.43\pm0.21)\cdot10^{12}$ m^{-2}	$(2.65\pm0.03)\cdot10^{13}m^{-2}$	$(1.40\pm0.10)\cdot10^{14}$ m^{-2}	$(2.43\pm0.52)\cdot10^{14}$ m^{-2}
Hardened 54SiCr6 steel	$(1.02\pm0.12)\cdot10^{16}$ m^{-2}	$(9.96\pm1.14)\cdot10^{15}$ m^{-2}	$(9.64\pm1.06)\cdot10^{15}$ m^{-2}	$(1.24\pm0.29)\cdot10^{16}$ m^{-2}	$(9.40\pm1.96)\cdot10^{15}m^{-2}$

The residual stress measurements for the two materials, hardened 54SiCr6 steel and pure Fe, revealed significant differences in their response to various surface preparation methods (Fig. 4). For the 54SiCr6 steel, grinding with P120 and P1200 sandpapers resulted in a high compressive residual stress near or below -1100 MPa, indicating that only grinding induces substantial compressive stress in the surface layer. Polishing with OPS colloidal silica leads to nearly neutral residual stress at -8 MPa, which implies that the polishing process relieves much of the compressive stress introduced by the grinding steps. On the other hand, after etching with HCl and electrolytic etching a slight tensile residual stress was detected, showing that chemical etching and electrolytic polishing induced minimal residual stress. For the pure Fe sample, the residual stresses after grinding with P120 and P1200 sandpapers indicated compressive residual stress around -300 MPa, though not as intense as in hardened 54SiCr6 steel. Polishing with OPS colloidal silica leads to a residual stress of -270 MPa, which was still compressive but less so than the grinding results. After etching with HCl, the tensile residual stress in pure Fe was -192 MPa, a lighter shift towards a tensile state compared to 54SiCr6, but still not as significant. Electrolytic etching in pure Fe resulted in a minimal residual stress of -23 MPa, similar to what was observed in 54SiCr6 steel.

The results presented above are focused on the influence of surface preparation methods on XRD analysis. One sample exhibited a ferritic microstructure with low hardness, whereas the second one displayed a martensitic microstructure with high hardness. After each grinding and polishing step, surface roughness was evaluated. In general, surface roughness decreased with decreasing abrasive particle size, followed by an increase after etching in HCl and electrolytic etching for both studied materials. The differences in surface roughness between pure Fe and hardened 54SiCr6 steel reflect the material's response to grinding and polishing processes, without a significant effect on diffraction peak characteristics, as reported in previous work [21]. The primary factor influencing peak broadening is the rate of plastic deformation, represented by increased dislocation density. As evident from Tab. 4, the effect of surface preparation on peak broadening is also strongly reflected in the dislocation density results calculated using the Williamson-Hall method. Furthermore, proper surface preparation is crucial for accurate phase composition determination. For example, evaluating retained austenite in quenched and tempered carbon steels can be challenging due to the overlap of martensite and austenite peaks, as described in [22]. Additional peak broadening caused by sample preparation would further complicate phase composition analysis.

Although the effect of surface preparation was more pronounced in the pure Fe samples likely due to the minimal initial distortions in the recrystallized ferrite structure-its influence on macroscopic residual stress measurements was significantly larger in the hardened 54SiCr6 steel sample.

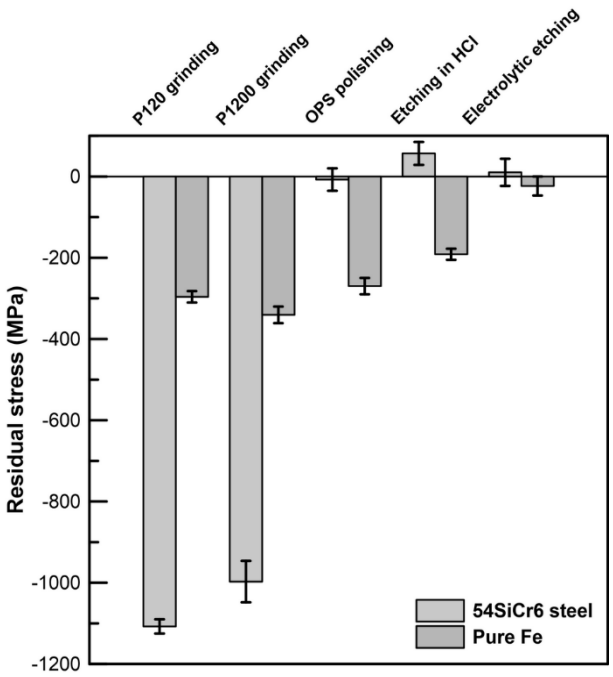

Fig. 4 *Impact of Surface Preparation on Residual Stress in hardened 54SiCr6 Steel and annealed pure Fe Samples*

4 Conclusions

This study demonstrates the crucial role of surface preparation of metallic samples in XRD analysis. The investigation was carried out on the sample with low hardness and recrystallized ferritic microstructure and on the hardened 54SiCr6 steel with martensitic microstructure.

- Influence on Diffraction Peak Characteristics: Mechanical grinding results in broader diffraction peaks due to surface-induced strain and deformation, in contrast to polished and etched samples. The samples with low hardness and ferritic microstructure were more sensitive to the final step of surface preparation.
- Residual Stress Analysis: Grinding induced significant compressive residual stresses, particularly in hardened 54SiCr6 steel (-1100 MPa), whereas chemical and electrolytic etching do not significantly influence the residual stress state.
- The surface preparation had a significant impact on the phase composition analysis of the hardened 54SiCr6 steel. After grinding with P120 and P1200 sandpapers, the intensities of austenite diffraction peaks were too low to determine the retained austenite content. The retained austenite content calculated over the full range of 30–125° 2θ yielded inconsistent results (11–16 wt.%) due to the overlap of martensite (110) and austenite (111) peaks, whereas the analysis from the limited range of 48–125° 2θ provided consistent results of approximately 8 wt.%. Differences in lattice parameters were most noticeable between samples prepared by grinding with P120 and P1200 and those prepared by OPS polishing, chemical etching, and electrolytic etching.
- A clear dependence of dislocation density on the sample polishing method for XRD measurement was observed for both pure iron and hardened 54SiCr6 steel. Sandpaper with large abrasive particles causes significant deformation of the sample and increases the number of crystalline defects. This affected layer is gradually removed in subsequent polishing steps, resulting in a decrease in dislocation density. For the steel under study, this effect is not as significant as for pure iron.

From the above findings, it follows that surface condition significantly impacts XRD analysis results, and improper sample preparation can greatly affect the accuracy of the analysis. Therefore, it is recommended to strictly adhere to the standardized surface preparation procedures as outlined in ASTM or ISO standards.

Acknowledgement

The development of this paper was financed by the institutional support for the long-term conceptual development of the research organization (Decision no. 3/2023 of the Ministry of Industry and Trade of the Czech Republic).

References

[1] KRATOCHVÍL, B., HUŠÁK, M., BRYNDA, J., SEDLÁČEK, J. (2008). What can the current X-ray structure analysis offer?. In: *Chemicke Listy,* Vol. 102, No. 10, pp. 889–901. ISSN 1213-7103

[2] KRATOCHVÍL, B., HUŠÁK, M., KOROTKOVA, E.I., JEGOROV A. (2016). The importance of x-ray crystal structure determinations for pharmacy. In: *Chemicke Listy,* Vol. 110, No. 1, pp. 40–47. ISSN 1213-7103

[3] KRAUS, I., GANEV, N. (2004). *Technické aplikace difrakční analýzy*, Vyd. 1, Publisher: CTU, Prague. ISBN 9788001030998

[4] LUŠTINEC, J., OČENÁŠEK, V. (2019). Residual Stresses and Cracks in Forgings of Heat-treatable Aluminium Alloys. In: *Manufacturing Technology,* Vol. 19, No. 4, pp. 637–643. ISSN 1213-2489

[5] BLATNICKÁ, M., ŠAJGALÍK, M., SÁGA, M., BLATNICKÝ, M. (2018). Comparison of Residual Stress in High Strength Steel Sample before and after Laser Welding. In: *Manufacturing Technology*, Vol. 18, No. 3, pp. 369–371. ISSN 1213-2489

[6] ANASIEWICZ, K., JÓZWIK, J., LELEŃ, M., PIEŚKO, P., LEGUTKO, S., TOMCZAK, J., PATER, Z., BULZAK, T. (2024). Identification of Internal Defects in Forged Shafts by Measurement of Residual Stresses Using X-Ray Method. In: *Manufacturing Technology,* Vol. 24, No. 5, pp. 711–720. ISSN 1213-2489

[7] DRAHOKOUPIL, J. (2011). *Interpretation of diffraction profiles, Doctoral thesis*, Czech Technical University in Prague, 2011.

[8] SHINTANI, T., MURATA, Y. (2011). Evaluation of the dislocation density and dislocation character in cold rolled Type 304 steel determined by profile analysis of X-ray diffraction, In: *Acta Materialia,* Vol. 59, No. 11, pp. 4314–4322. ISSN 1359-6454

[9] WEI, Y., YU, X., HAO, T., YANG, S., SU, Y., ZHAO, W. (2024). Effect of the Surface Carbon Content on Mi-crostructure and Deformation of M50 Steel. In: *Journal of Materials Engineering and Performance,* Vol. 33, No. 15, pp. 7990–7997. ISSN 1059-9495

[10] MUIRURI, A., MARINGA, M., DU PREEZ, W. (2020). Evaluation of Dislocation Densities in Various Micro-structures of Additively Manufactured Ti6Al4V (Eli) by the Method of X-ray Diffraction. In: *Materials*, Vol. 13, No. 23, pp. 5355. ISSN 1996-1944

[11] CHEN, Y., SUN, H., LI, Z., WU, Y., XIAO, Y., CHEN, Z., ZHONG, S., WANG, H. (2020). Strategy of Residual Stress Determination on Selective Laser Melted Al Alloy Using XRD. In: *Materials*, Vol. 13, No. 2, pp. 451. ISSN 1996-1944

[12] BARROW, A.T.W., KANG, J.-H., RIVERA-DÍAZ-DEL-CASTILLO, P.E.J. (2012). The $\epsilon \rightarrow \eta \rightarrow \theta$ transition in 100Cr6 and its effect on mechanical properties. In: *Acta Materialia*. Vol. 60, No. 6-7, pp. 2805–2815. ISSN 1359-6454

[13] PAGLIARO, P., PRIME, M.B., ROBINSON, J.S., CLAUSEN, B., SWENSON, H., STEINZIG, M., ZUCCARELLO, B. (2011). Measuring Inaccessible Residual Stresses Using Multiple Methods and Superposition, In: *Experimental Mechanics*. Vol. 51, No. 7, pp. 1123–1134. ISSN 0014-4851

[14] KLEMM-TOOLE, J., BENZ, J., VIEIRA, I., CLARKE, A.J., THOMPSON, S.W., FINDLEY, K.O. (2020. Strengthening mechanisms influenced by silicon content in high temperature tempered martensite and bainite. In: *Materials Science and Engineering: A*, Vol. 786, pp. 139419. ISSN 0921-5093

[15] YAZDANMEHR, A., JAHED, H. (2020) On the Surface Residual Stress Measurement in Magnesium Alloys Using X-Ray Diffraction. In: *Materials,* Vol. 13, No. 22, pp. 5190. ISSN 1996-1944

[16] LUKAS, M., MAYER, M., STARK, A., FRIESSNEGGER, B., HÖNIGMANN, T., GALLER, M., RESSEL, G. (2022). Influence of Tempering on Macro- and Micro-Residual Stresses and Yield Stress of Ferritic-Pearlitic Drawn, Coiled, and Straightened Wires. In: *Metallurgical and Materials Transactions A*, Vol. 53, No. 11, pp. 3977–3985. ISSN 1073-5623

[17] E468-18; Practice for X-RAY Determination of Retained Austenite in Steel with Near Random Crystallographic Orientation. ASTM International: West Conshohocken, PA, USA, 2013.

[18] RIETVELD, H.M. (1969). A profile refinement method for nuclear and magnetic structures. In: *Journal of Applied Crystallography*, Vol. 2, No. 2, pp. 65–71. ISSN 0021-8898

[19] UNGÁR, T., BORBÉLY, A. (1996). The effect of dislocation contrast on x-ray line broadening: A new ap-proach to line profile analysis. In: *Applied Physics Letters,* Vol. 69, No. 21, pp. 3173–3175. ISSN 0003-6951

[20] UNGÁR, T., DRAGOMIR, I., RÉVÉSZ, Á., BORBÉLY, A. (1999). The contrast factors of dislocations in cubic crystals: the dislocation model of strain anisotropy in practice. In: *Journal of Applied Crystallography*. Vol. 32, No. 5, pp. 992–1002. ISSN 0021-8898

[21] AMANOV, A., YEO, I.K., JEONG, S.H. (2025). Advanced post-processing of Ti–6Al–4V alloy fabricated by selective laser melting: A study of laser shock peening and ultrasonic nanocrystal surface mod-ification. In: *Journal of Materials Research and Technology,* Vol. 35, pp. 4020–4031. ISSN 2238-7854

[22] KUMAR, S., SINGH, S.B. (2023). Quantification of Retained Austenite in Low-Carbon Steels. In: *Metallurgi-cal and Materials Transactions A,* Vol. 54, No. 11, pp. 4283–4294. ISSN 1073-5623